Adaptive Stator Ground Fault Protection for Variable Speed Operation of Synchronous Machines

Kumar Mahtani, José M. Guerrero, Luis F. Beites, and Carlos A. Platero

To cite this version:

K. Mahtani, J. M. Guerrero, L. F. Beites and C. A. Platero, "Adaptive Stator Ground Fault Protection for Variable Speed Operation of Synchronous Machines," in IEEE Transactions on Industry Applications, vol. 61, no. 5, pp. 7061-7071, Sept.-Oct. 2025, doi: 10.1109/TIA.2025.3559024.

Published Version.

Published 2025 September 01

Archivo Digital UPM houses in digital format the academic and scientific documentation (theses, pfc, articles, etc.) generated at the institution and makes it accessible through the Internet, within the framework of the Budapest Open Access Initiative and the Berlin Declaration, of which the Universidad Politécnica de Madrid is a signatory.

El **Archivo Digital UPM** alberga en formato digital la documentación académica y científica (tesis, pfc, artículos, etc..) generada en la institución y la hace accesible a través de Internet, en el marco de la Iniciativa por el Accesso Abierto de Budapest y la Declaración de Berlín, de la que es signataria la Universidad Politécnica de Madrid.

This article has been accepted for publication in IEEE Transactions on Industry Applications. This is the author's version which has not been fully edited and content may change prior to final publication. Citation information: DOI 10.1109/TIA.2025.3559024

Adaptive Stator Ground Fault Protection for Variable Speed Operation of Synchronous Machines

Kumar Mahtani, José M. Guerrero, *Member*, *IEEE*, Luis F. Beites, and Carlos A. Platero, *Senior Member*, *IEEE*

***Abstract*— Synchronous machines usually operate at constant speed in power systems. However, there are specific applications, such as the generators used in diesel-electric transmissions or Type 4 wind turbines, that operate at variable speed. These machines are provided with various protective relaying functions depending on their rated power and service type, including conventional fixed-setting stator-ground fault (SGF) protection. However, under variable speed conditions, SGF protection with fixed settings often fails to protect the stator winding across the full operating range and may also lead to unintended tripping due to improper harmonic filtering. This paper presents an adaptative SGF protection method for SMs operating at variable speed. The proposed system dynamically adjusts the tripping threshold to the machine's operating frequency, ensuring comprehensive protection. Extensive simulations and experimental tests validate the effectiveness of the proposed protection method, yielding promising results.**

***Index Terms*— AC generators, Alternators, Fault protection, Grounding, Protective relaying, Power system faults, Power system protection, Stator windings, Stators, Synchronous machines.**

NOMENCLATURE

α	Stator winding protection percent coverage
f	Fundamental frequency
R_f	Fault resistance
R_{gnd}	Grounding resistance
$t_0>$	Time delay
$\underline{U}$, U	Line-to-line voltage raw signal and RMS value
$\underline{U}_i$, U_i	Phase 'i' voltage signal and RMS value
$\underline{U}_{ij}$, U_{ij}	Line voltage between phases "i" and "j" signal and RMS value
U_n	Rated voltage (RMS value, line-to-line)
U_f	Line-to-line voltage at f frequency (RMS value)
$\underline{U}_{gnd}$, U_{gnd}	Ground voltage raw signal and RMS value
$U_{gnd,trip}$	Tripping threshold/pick-up value
$\underline{U}_{gnd,f}$, $U_{gnd,f}$	Ground voltage at f frequency signal and RMS value
$U_{gnd,f,trip}$	Tripping threshold/pick-up value at f frequency
$U_0>$	Minimum detectable percentual fault location
x	Fault position

I. INTRODUCTION

SYNCHRONOUS machines (SMs) are the most prominent electrical machines used in power generation. Among the various electrical faults that can occur in these machines, stator ground faults (SGFs) are particularly prevalent and pose significant operational risks [1]. The zero-sequence impedance of SMs is typically around half of their positive sequence subtransient reactance, resulting in per-phase fault currents during a single SGF that can exceed those in three-phase faults without proper grounding [2]. This characteristic amplifies the potential damage to the stator windings and core, making SGFs particularly hazardous. Although symmetrical faults are commonly addressed in industrial standards and design protocols, SGFs demand special attention due to their disproportionate impact on machine integrity and reliability. The ability to detect and mitigate SGFs is thus essential for ensuring the longevity and safety of SMs in power systems.

SGFs are frequently the result of insulation degradation in the stator windings, which can be triggered by internal or external events such as sudden faults, voltage surges, or transient overvoltages that exceed the insulation's withstand capacity. The degradation process can be driven by electrical, thermal, mechanical, or environmental stressors [3]. Over time, these factors gradually weaken the insulation, increasing the likelihood of an SGF if not detected and mitigated in its early stages. Detecting the first SGF is crucial due to the severe consequences that could arise from a second SGF, which could result in a direct phase-to-phase short circuit, i.e., a condition unimpeded by grounding impedance. This underlines the critical importance of early SGF detection to prevent catastrophic damage and ensure the ongoing reliability of the machine.

To mitigate the risks associated with high transient overvoltages in ungrounded generators, which can lead to insulation breakdown, and to prevent the excessive fault currents in directly grounded generators, a common trade-off solution is the implementation of high-impedance groundings [4]. As illustrated in Fig. 1, high impedance grounding can be achieved by placing either a grounding resistor (Fig. 1a) or a single-phase distribution transformer with a low-voltage grounding resistor (Fig. 1b) between the stator neutral point and ground [5]-[6].

K. Mahtani, L. F. Beites, and C. A. Platero are with the Department of Automation, Electrical and Electronic Engineering and Industrial Informatics, Escuela Técnica Superior de Ingenieros Industriales, Universidad Politécnica de Madrid, 28006 Madrid, Spain (e-mails: kumar.mahtani@upm.es; luis.fbeites@upm.es; carlosantonio.platero@upm.es).

J. M. Guerrero is with the Department of Electrical Engineering, Escuela de Ingeniería de Bilbao, Universidad del País Vasco-Euskal Herriko Unibertsiatea, 48013 Bilbao, Spain (e-mail: josemanuel.guerrerog@ehu.eus).

This work is licensed under a Creative Commons Attribution 4.0 License. For more information, see https://creativecommons.org/licenses/by/4.0/

This article has been accepted for publication in IEEE Transactions on Industry Applications. This is the author's version which has not been fully edited and content may change prior to final publication. Citation information: DOI 10.1109/TIA.2025.3559024

In any of the grounding configurations, traditional protection functions [7]-[8] typically include an overvoltage relay (ANSI 59N), also known as neutral voltage displacement relay, installed at the grounding resistor or on the secondary side of the distribution transformer. Another prevalent approach involves the use of an overcurrent relay (ANSI 51N) placed either between the neutral point and ground or on the secondary side of the distribution transformer. These protection functions are generally tuned to cover approximately 95% of the winding, as observed from the terminal opposite the neutral point ($\alpha = 95$ %).

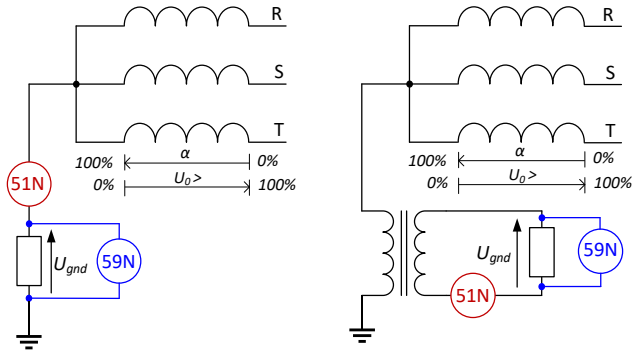

Fig. 1. SM grounding configurations with conventional protective relaying functions [(a): High voltage grounding resistor; (b): Distribution transformer and low voltage resistor].

Both protective relaying functions (ANSI 59N or ANSI 51N) incorporate harmonic filters designed to eliminate the influence of the harmonics, usually the third harmonic. This capability enables the relays to accurately detect voltages or currents at the fundamental frequency while preventing unwanted trips due to harmonic distortion. Furthermore, frequency-selective grounding impedance designs have been proposed [9], which function as solid grounding for high-frequency harmonics while acting as low-resistance grounding for low-frequency signals. The mentioned protections are often supplemented by differential protection schemes [10], such as full differential protection (ANSI 87N) or restricted earth fault protection (ANSI 64REF).

Particularly for low-power machines, it is often assumed that SGFs occurring in the lower winding portions do not result in significant damage; therefore, this 95% coverage may suffice as the sole protective element. In such cases, winding tests during outages are conducted to detect potential faults in the lower portion. Although advancements in offline SGF detection methods have been made [11]-[12] to address the limitations of traditional techniques, such as the golden search method, these methods require the machine to be taken out of service to conduct diagnostics.

However, when complete winding protection is required, especially for high-power machines, other schemes are added to supplement zero-sequence voltage schemes, such as low frequency injection (ANSI 64S) [13]-[15], that requires additional sources, circuitry and control algorithms, third-harmonic protection schemes such as neutral undervoltage (ANSI 27TN) or voltage differential (ANSI 59THD) [16]-[17]. Most of these protections are highly dependent on machine design, particularly the stator winding pitch and loading conditions. In this sense, recent advances have adapted third-harmonic schemes to address their limitations at low load conditions [18]-[19].

However, all the mentioned SGF protection functions operate with fixed settings based on system-rated frequency and voltage, as these protective relaying systems are generally designed for SMs coupled to electrical power systems that maintain nearly constant frequency and voltage. Consequently, there is a significant gap in SGF protection for SMs operating under variable speed conditions, involving loss of winding coverage and improper filtering, as addressed in Section II. The inability of the conventional SGF protection to adapt to these dynamic conditions poses a risk to the safety of SMs, highlighting the need for innovative protective solutions that can adjust to varying operational parameters.

The mentioned protection gap, covered by this work, is particularly relevant for converter-interfaced SMs, largely utilized in diesel-electric propulsion systems such as those used in locomotives and vessels, and Type-4 wind power conversion systems, among other applications.

To address this protection gap, this paper introduces a self-adaptive SGF protection function for SMs operating at variable speeds [20][21]. This innovative solution was granted a patent [21]. While [20] presented the theoretical framework and initial feasibility of the approach, this work strengthens the technical foundation and provides extensive validation through improved simulations and experimental testing across a wide range of fault resistances, winding locations, and machine operating speeds. The experimental studies were conducted on an ad-hoc SM equipped with stator taps.

The main contribution of the proposed method involves the real-time adjustment conditions of the SGF protection to the machine's operating, avoiding the problems that arise in this protection at off-rated operating speeds (winding protection coverage reduction and miss-filtering of the fundamental frequency). By avoiding the mentioned issues, this approach ensures that the fault detection capabilities for any operating speed equalize those for the rated speed. Moreover, the proposed method can be implemented without the need for additional equipment, neither any type of signal injection technique, as only software developments in conventional digital relays are required. The innovation focuses on robustness, simplicity, and cost-effectiveness to facilitate industrial adoption.

The present work is structured as follows. Section II describes the limitations of conventional SGF protection functions. Section III outlines the operational principles of the proposed method. Section IV presents the simulation results, while Section V details the experimental validation. Finally, Section VI concludes by summarizing the main contributions of the work and suggesting future research directions in this area.

II. Problem Statement

Conventional SGF protections, which utilize overvoltage (ANSI 59N or 59G) or overcurrent (ANSI 51N or 51G) relays,

This work is licensed under a Creative Commons Attribution 4.0 License. For more information, see https://creativecommons.org/licenses/by/4.0/

This article has been accepted for publication in IEEE Transactions on Industry Applications. This is the author's version which has not been fully edited and content may change prior to final publication. Citation information: DOI 10.1109/TIA.2025.3559024

are based on the linear relationship between the voltage or current measurements acquired by the relay and the fault location within the stator winding. This linear relationship is theoretically valid under the assumption that the stator's series impedance and grounding capacitances are negligible in the analysis of fault current flow, particularly because the grounding resistance is typically in the kΩ range. Theoretically, the parasitic current flow associated with ground capacitances within the zero-sequence circuit shall be analyzed in order set the minimum pick-up or threshold voltage ($U_{gnd,trip}$) required to avoid false tripping due to faults beyond the protection zone (for example, at the grid side of the generator transformer). In practice, $U_{gnd,trip}$ is typically set at 5% of $U_n/\sqrt{3}$ and the grounding resistor (R_{gnd}) is usually sized to limit fault currents to 5 or 10 A in the worst-case SGF scenario (solid SGF at terminals). The voltage impressed at the grounding resistor for a solid SGF at point x with fault resistance R_f is given by (1).

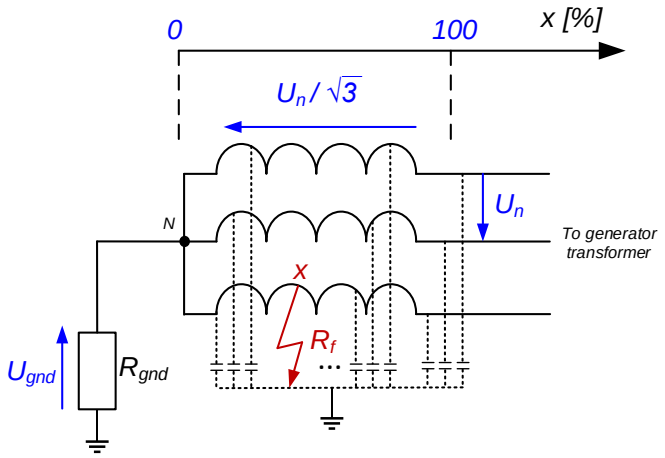

Fig. 2. Representation of a solid SGF produced at point x.

$$U_{gnd} = \frac{R_{gnd}}{R_{gnd} + R_f} \cdot x \cdot \frac{U_n}{\sqrt{3}} \quad (1)$$

The maximum winding protection percentage coverage (U_0>) is a critical metric, which is related to the least severe protected solid SGF, i.e. the operable SGF closest to the stator neutral point (α) with $R_f = 0$. The stator winding coverage is calculated as per (2):

$$\alpha = \frac{\left(U_n/\sqrt{3} - U_{gnd,trip}\right)}{U_n/\sqrt{3}} \cdot 100 = 100 - U_0\rangle \quad (2)$$

For typical capacitance values in synchronous generators, $U_{gnd,trip}$ usually represents less than 5% of $U_n/\sqrt{3}$. Therefore, as mentioned, [U_0>] = 5%, i.e. α = 95% is generally accepted as a trade-off between sensitivity and reliability in fault detection and tripping. This implies that the protective function will not detect any SGF occurring within the initial 5% of the winding on the neutral point side. For coordination purposes, a tripping delay is usually set for this protective function. Additionally, a second overvoltage protective element may be incorporated, featuring a higher threshold setting and a shorter tripping delay to provide an extra layer of protection.

These protection functions typically operate with fixed settings, which raises significant concerns regarding their performance under off-rated frequency conditions, often well below its rated speed. In these applications, it is anticipated that the machine's output voltage varies linearly with speed in order to prevent overfluxing, following a constant V/Hz control strategy.

The theoretical basis of the conventional fixed-setting protection scheme for rated speed is depicted in Fig. 3. Under constant V/Hz excitation control, the generator voltage is proportionally reduced in relation to the frequency, resulting in the protection operating within a linear framework. This is further illustrated in Fig. 3, which depicts the grounding voltage (U_{gnd}) as a function of fault location (x) when operating at a speed lower than the rated (therefore $U < U_n$), which is linear according to (1). It is deduced that because the pick-up setting is fixed by the conventional scheme, the winding protection coverage is reduced ($\alpha' < \alpha$) at speeds below the rated value [21].

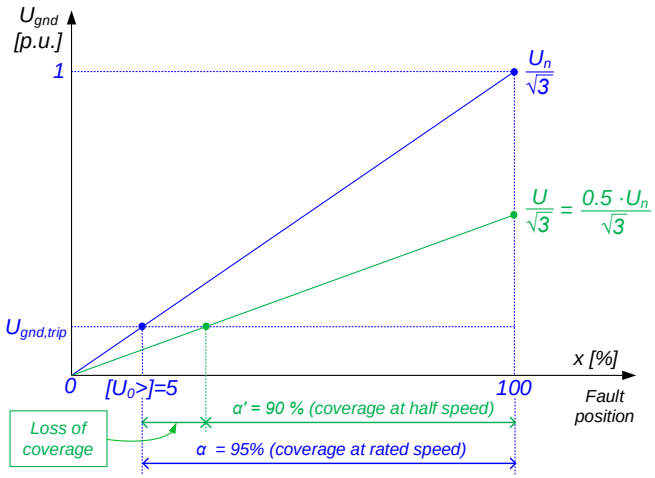

Fig. 3. Grounding voltage [p.u.] with respect to fault position [%]: Conventional tripping scheme (blue) and tripping scheme for a 50% reduced speed (green).

Fig. 3 is presented in a per-unit (p.u.) system, with $U_n/\sqrt{3}$ as the base voltage. For a specified pick-up voltage ($U_{gnd,trip}$), the loss of protection is represented by the horizontal distance between the characteristics at the $U_{gnd,trip}$ ordinate. The loss of protection is linear with the variation in speed, which correlates with changes in the operating voltage. As example in Fig. 3, when the operating voltage is reduced to half its rated value ($U = 0.5 \cdot U_n$), the length of the winding without protection coverage can double, reaching 10% ($\alpha' = 90\%$). Furthermore, if the operating voltage falls below the fixed pick-up voltage ($U/\sqrt{3} < U_{gnd,trip}$), the entire winding becomes unprotected. This situation highlights a critical lack of protection during machine operation at reduced voltage levels. The expression for the maximum winding protection percentage coverage at any speed different from the rated speed, corresponding to the output

This work is licensed under a Creative Commons Attribution 4.0 License. For more information, see https://creativecommons.org/licenses/by/4.0/

This article has been accepted for publication in IEEE Transactions on Industry Applications. This is the author's version which has not been fully edited and content may change prior to final publication. Citation information: DOI 10.1109/TIA.2025.3559024

phase voltage $U_{gnd,trip} \leq U/\sqrt{3} \leq U_n/\sqrt{3}$, is given by (3):

$$\alpha' = \frac{U/\sqrt{3} - U_{gnd,trip}}{U/\sqrt{3}} \cdot 100 \quad (3)$$

It should be noted that (2) and (3) are equally valid for frequency or speed instead of voltage, assuming constant flux control. Similarly, the application of these expressions within a p.u. system would be analogous for voltage, frequency, or speed, allowing for consistent analysis across different operational conditions.

The 95% ground fault protection scheme is based on the fundamental frequency of the measured voltage or current. However, SMs can generate significant harmonic content under healthy conditions, particularly with triple harmonics for 5/6 pitch windings (3rd, 9th, 15th, etc.), where the 3rd harmonic generally accounts for the largest contribution. These harmonics generally exhibit similar magnitudes and phase angles across all three phases. In the case of 2/3 pitch windings, the 5th and 7th harmonics are expected to be notably amplified and triple harmonics to be canceled. Consequently, relaying functions must effectively filter out any harmonic components other than the fundamental frequency, which raises concerns in variable frequency operation. The issue of miss-filtering is illustrated in Fig. 4, demonstrating a bandpass filtering approach when the fundamental operating frequency (f') is lower than the reference frequency (f). This scenario emphasizes the necessity of accurate frequency tracking to ensure proper tuning of the protection functions at the fundamental frequency [21].

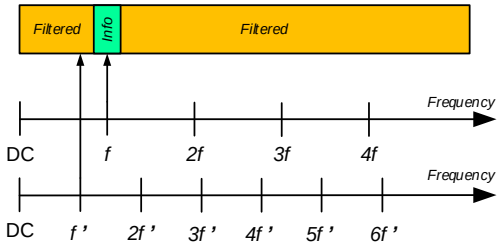

Fig. 4. Miss-filtering when operating at a lower frequency (f') than the tuned.

III. Operational Principles of the Proposed SGF Protection Method

This section outlines the operational principles of the proposed protection function [20], using an overvoltage relay (ANSI 59N) in a grounding resistor configuration for illustrative purposes. However, the underlying principles of the protection scheme are versatile and can be extended to overvoltage relays in a grounding distribution transformer configuration, as well as to overcurrent protection (ANSI 51N) in any grounding configuration. A schematic representation of the proposed method is provided in Fig. 5.

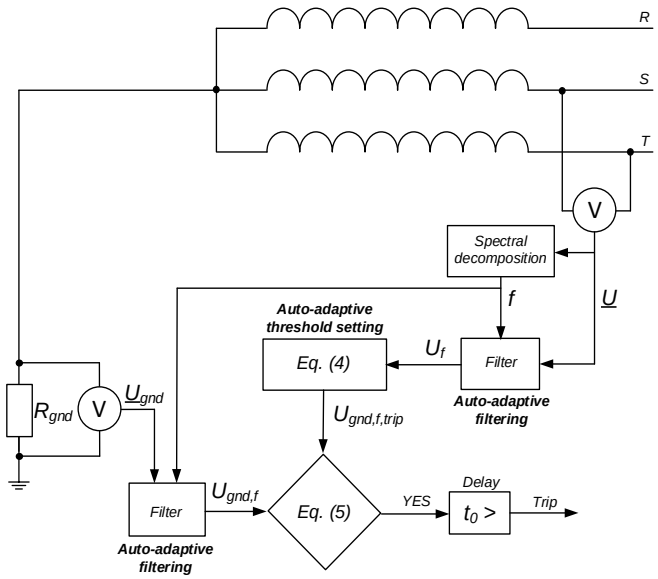

Fig. 5. Schematic layout of the proposed SGF protection method.

To obtain real-time operational features, a line voltage signal, $\underline{U}$, measured at the machine's output terminals, is utilized as input for the proposed method. This approach is chosen in order to avoid measurement distortions caused by neutral displacement in the event of an SGF, as depicted in Fig. 6. From the measured line voltage signal, the fundamental frequency, f, corresponding to the operating speed, is extracted along with its magnitude (RMS value), U_f. This is accomplished through auto-adaptive filtering techniques. In general, the extraction of f from $\underline{U}$ can be achieved by means of the Fast Fourier Transform (FFT) or other harmonic decomposition techniques. However, for the particular case of constant V/Hz excitation control strategy, the extraction of the fundamental frequency from $\underline{U}$ can be largely simplified given the direct relationship with its magnitude. Alternatively, the velocity signal from the encoder, if available, or even the frequency setpoint from the drive's phase-locked loop (PLL), can also be used to filter the first harmonic.

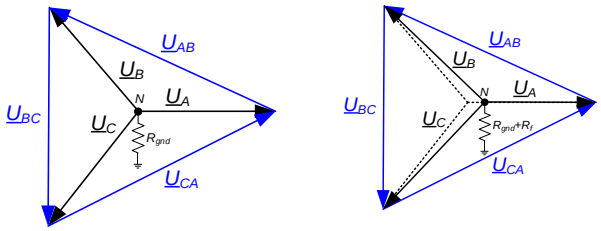

(a) (b)

Fig. 6. Phasor representation of phase and line voltages [(a): Healthy condition; (b) Neutral displacement in the case of an SGF].

Then, the tripping threshold, $U_{gnd,f,trip}$, is dynamically adjusted in real-time to align with the operating voltage or speed, according to (4):

$$U_{gnd,f,trip} = U_0\rangle \cdot \frac{U_f}{\sqrt{3}} \quad (4)$$

This work is licensed under a Creative Commons Attribution 4.0 License. For more information, see https://creativecommons.org/licenses/by/4.0/

This article has been accepted for publication in IEEE Transactions on Industry Applications. This is the author's version which has not been fully edited and content may change prior to final publication. Citation information: DOI 10.1109/TIA.2025.3559024

This computation enables an auto-adaptive threshold setting that adjusts in real-time according to the machine's operating conditions at each time. The parameter $U_0>$ in (4) allows for the selection of the location of the least severe fault to be protected, with $[U_0>] = 0$ at the neutral point and $[U_0>] = 100\%$ at the opposite end of the stator winding. However, as an excessive reduction in $U_0>$ negatively impacts the selectivity of the protection function, as discussed in Section II, it is common practice to protect 95% of the stator winding, which corresponds to $[U_0>] = 5\%$.

In addition, the voltage across the grounding resistor, $\underline{U}_{gnd}$, measured between the machine's neutral point and ground, is continuously monitored. The RMS magnitude of the grounding voltage component at the operating frequency, $U_{gnd,f}$, is extracted also through auto-adaptive filtering, implying that harmonic components other than the fundamental frequency (notably triple harmonic components) are filtered out from $\underline{U}_{gnd}$. The value of $U_{gnd,f}$ is negligible in the absence of an SGF, but increases when a SGF occurs, with its magnitude directly proportional to the fault location along the stator winding, as described in Section II. The protection function initiates a trip when the condition stated in (5) is met:

$$U_{gnd,f} > U_{gnd,f,trip} \tag{5}$$

The tripping signal generated by the proposed protection method can be subjected to a time-delay characteristic ($t_o>$), to ensure proper coordination with other protection systems. This time delay helps avoid unwanted or premature tripping, preventing unnecessary disconnections due to transient conditions or disturbances that could trigger a false positive.

The proposed method does not require additional hardware compared to conventional SGF protection schemes. Specifically, it relies on standard measurements of neutral grounding voltage ($\underline{U}_{gnd}$) and armature voltage ($\underline{U}$), both of which are routinely monitored in digital protection relays. The operating frequency (f) is derived directly from $\underline{U}$. The lack of additional hardware minimizes the installation complexity and cost.

Although in this work the proposed method has been designed for its implementation in conventional digital relays, it can also be implemented within the inverter control system, simplifying the operating frequency extraction at the cost of enabling an additional input for the neutral voltage measurement.

On the other hand, implementing the adaptive functionality requires additional software capabilities within digital relays, for real-time filtering and dynamic adjustment of the tripping threshold ($U_{gnd,f,trip}$). Specifically, regarding the real-time frequency filtering capabilities, it is worth noting that, in practice, prior spectral decomposition performed using the FFT or other decomposition technique is required, over a running window of at least one cycle of the fundamental frequency. This auto-adaptive filtering capacity is essential to prevent improper filtering, as illustrated in Fig. 4. The possibility of unintended trips due to misinterpretation is avoided (see for example $f' = f/3$ in Fig. 4). The system continuously adapts its filtering process to match the operating conditions.

In essence, by only upgrading the software associated with the SGF protection utilized in conventional digital relays, SGFs can be reliably detected throughout the entire stator winding for any operating speed, improving the conventional SGF protection. The computational capabilities required for the implementation of the proposed method are suited for the processing platforms of modern digital relays, ensuring cost-effective integration.

IV. Computer Simulations

This section describes the computer simulations conducted to validate the proposed auto-adaptive SGF protection method. The simulations were implemented in the MATLAB/Simulink environment to evaluate the method's performance across various operating scenarios. These scenarios included different SGF at different locations (x = 2.5, 5, 7.5 and 10%, all near the neutral point), with varying fault resistances (ranging from R_f = 0, 10 and 100 Ω, to higher values like 1 and 10 kΩ, to assess the method's sensitivity to varying fault severities), under various machine operating speeds (1800, 1350, 900, and 450 rpm), i.e., various operating frequencies (f = 180, 135, 90 and 45 Hz).

The simulation model featured a 12-pole, 1850-kVA, 2.6-kV, 180-Hz (1800 rpm) SM operating under variable speed conditions. The rated parameters of the tested SM are provided in Table I. The SM was modelled with detailed electrical and mechanical characteristics to replicate realistic behaviour under variable speed conditions. The stator winding was represented with distributed parameters (resistance, leakage reactance, and mutual reactance), while parasitic ground capacitances were modelled explicitly to account for their impact on zero-sequence currents and voltages. Access was enabled to the stator winding at different points to perform ground faults, allowing for a granular evaluation of the method's performance. Faults were performed with varying fault resistances, to assess the sensitivity and reliability of the method. The rotor was modelled with a standard d-q axis representation, capturing the effects of field excitation and damper windings.

TABLE I

Rated Values of the Simulated SM

Type of machine	Synchronous 3-phase	
Rated power	1850	kVA
Rated voltage	2600	V
Rated frequency	180	Hz
Rated speed	1800	rpm
Pole pairs	6	
Rated current	410	A
Field excitation voltage	180	V
Field excitation current	1100	A
Stator resistance	0.004	Ω
Stator leakage reactance	0.1	pu
Rotor d-axis reactance	1.7	pu
Rotor q-axis reactance	1.55	pu
Grounding resistor	300	Ω
Grounding capacitance (per-phase)	10	μF
Moment of inertia	500	kg·m^2

To emulate a diesel-electric powertrain accurately, the machine's shaft dynamics were included, representing the inertia and damping effects. To replicate realistic power consumption of a diesel-electric powertrain, the SM was loaded with a full AC/DC converter, a smoothing capacitor and a DC

This work is licensed under a Creative Commons Attribution 4.0 License. For more information, see https://creativecommons.org/licenses/by/4.0/

This article has been accepted for publication in IEEE Transactions on Industry Applications. This is the author's version which has not been fully edited and content may change prior to final publication. Citation information: DOI 10.1109/TIA.2025.3559024

resistive load, ensuring that the machine's output voltage and current were aligned with those observed in practical applications. All signals were sampled at 20 kHz, ensuring that at least 100 samples per cycles were acquired at the highest operating frequency of 180 Hz.

The constant V/Hz control strategy, typically utilized in these applications, was employed to ensure constant flux linkage throughout variable speed operation. A [U_0>] = *0.05* setting was selected to protect 95% of the stator winding. Accordingly, a high-impedance grounding resistor R_{gnd} = 300 Ω was used to limit the fault current to 5 A in the most severe SGF scenario (a direct ground fault at x = 100 % for the rated speed operation), ensuring that the fault conditions were representative of actual power system configurations.

Steady-state machine operation was considered, at the mentioned operating frequencies (f = 180, 135, 90 and 45 Hz). Given the fault current limitation provided by the use of R_{gnd}, the action of the protection system can be delayed by a few cycles without compromising safety. Thereby, the diagnostic can be safely performed when the machine achieves steady-state operation, ensuring accuracy and avoidance of transient noise. Furthermore, in the context of diesel-electric traction, constant speed operation during relatively long sections is a prominent situation.

The proposed SGF protection function was implemented with auto-adaptive filtering mechanisms to extract the fundamental frequency and RMS voltage from the terminal and grounding voltage signals. The system continuously tracked the fundamental frequency in real time and adjusted the tripping threshold accordingly. Fault detection capabilities were tested, focusing on the method's ability to adapt to speed variations, providing consistent protection coverage across the entire operational range.

The performance of the proposed protection method was compared with the conventional 95 % SGF protection using a fixed setting for 50 Hz. In the proposed method, the tripping threshold of the grounding resistor voltage, $U_{gnd,f,trip}$, was automatically adjusted in real-time following (4), while the conventional protection function used a fixed threshold, $U_{gnd,trip}$, previously set based on (2).

A detailed example for an SGF executed at t = 1 s in phase '*a*' at x = *7.5 %* with R_f = 0 (solid fault) is illustrated in Figs. 7 and 8. Fig. 7 shows a line voltage ($\underline{U}$ = $\underline{U}_{ab}$), as well as the RMS value of the fundamental frequency component extracted from $\underline{U}$ and its RMS value, U_f, from which the tripping threshold is computed: 2.6 kV for the rated speed (1800 rpm) and 1.3 kV for half the rated speed (900 rpm). From Fig. 7, it is evident that, unlike the phase voltage, the line voltage is not impacted by the displacement of the neutral reference after the fault. Moreover, the V/Hz excitation control method yields linear variations of voltage with speed, as evidenced in Fig. 7. It should be noted that, due to the machine design (5/6 pitch winding), the output voltage at the machine terminals exhibits a highly distorted waveform with sharp notches and uneven sections, mainly corresponding to triple harmonics (3rd and 9th).

For an off-rated speed corresponding to half the rated speed (900 rpm), Fig. 8 illustrates the raw voltage signal captured at the grounding resistor terminals, $\underline{U}_{gnd}$, its fundamental frequency component obtained through a trailing FFT, $\underline{U}_{gnd,f}$, and its RMS value computed over a running average window of one cycle of the fundamental frequency, $U_{gnd,f}$. As depicted in Fig. 8, for [U_o>] = 5%, (4) yields approximately $U_{gnd,f,trip}$ = 37.52 V, while (2) provides approximately $U_{gnd,trip}$ = 75 V for any operating speed. Both the auto-adaptive threshold and the conventional fixed threshold are depicted in Fig. 8.

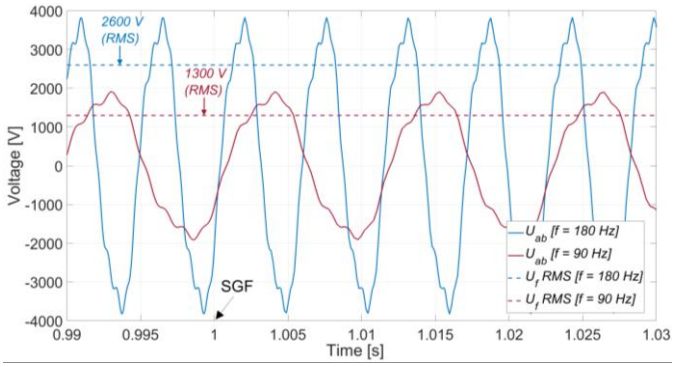

Fig. 7. Simulation results. Measured terminal voltage ($\underline{U}$=$\underline{U}_{ab}$) and RMS value for the fundamental frequency (U_f) extracted from the auto-adaptive filtering, for the rated speed (1800 rpm; 180 Hz) and half the rated speed (900 rpm; 90 Hz). The SGF is executed at t = 1 s.

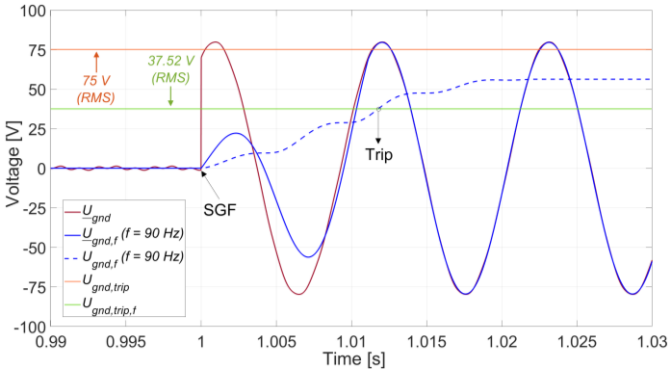

Fig. 8. Simulation results for an SGF at x = 7.5 % with R_f = 0 (solid fault) under [90 Hz, 1300 V] operating conditions.

According to Fig. 8, before the SGF execution $\underline{U}_{gnd}$ reflects the voltage impressed across the grounding resistor related to parasitic current leakage due to winding ground capacitance under normal conditions. These values, which are negligible compared with the faulty cases, impose the minimal operable adaptive threshold setting in order to avoid false tripping. When the SGF is executed, the voltage across the grounding resistor rises sharply following the closure of the low-impedance ground fault circuit. This signal is consistent with the voltage applied to the fault circuit, reaching peak values of 80 V. After the fault, the dynamically-computed $\underline{U}_{gnd,f}$ stabilizes in magnitude and phase after one complete trailing window computation, corresponding to one cycle of the fundamental frequency. Calculating the RMS value of $\underline{U}_{gnd,f}$ requires at least one more complete cycle, resulting in an additional one-cycle delay until its steady state value (56.5 V_{RMS}). However, considerably before this calculation lag, shortly after the first fundamental frequency cycle, the tripping condition described in (5) is met, as $U_{gnd,f}$ exceeds $U_{gnd,f,trip}$. In contrast, the conventional tripping threshold is set significantly above the steady state value of $U_{gnd,f}$ for these operating conditions, causing the SGF to remain undetected by the conventional protection method. The proposed auto-adaptive threshold enables timely SGF detection, which would otherwise go unnoticed under the analogous [U_o>] = 5% fixed setting.

Analogously, Fig. 9 shows the evolution of $U_{gnd,f}$ over time for different R_f values, for the same SGF in phase '*a*' at x = *7.5*

This work is licensed under a Creative Commons Attribution 4.0 License. For more information, see https://creativecommons.org/licenses/by/4.0/

This article has been accepted for publication in IEEE Transactions on Industry Applications. This is the author's version which has not been fully edited and content may change prior to final publication. Citation information: DOI 10.1109/TIA.2025.3559024

% for the operating speed of 900 rpm. It is demonstrated that such SGF at half speed cannot be detected by conventional protecting relaying functions for any fault resistance R_f, not even for a solid ground fault (R_f = 0). In contrast, the proposed auto-adaptive threshold setting successfully detects the SGFs with fault resistances of R_f = 0, 10 and 100 Ω. However, for very high-impedance, thus less severe ground faults, such as R_f = 1 and 10 k Ω, the fault remains undetected. Additionally, as illustrated in Fig. 9, the fault detection or pick-up time is directly related to the fault resistance, reaching its minimum for R_f = *0*, which, in this case, corresponds to 7.52 ms.

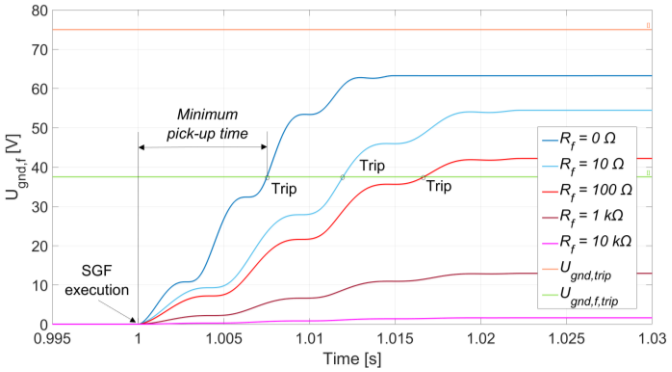

Fig. 9. Simulation results. Evolution of $U_{gnd,f}$ over time for an SGF at x = 7.5 % with different fault resistances R_f under [90 Hz, 1300 V] operating conditions.

Moreover, by applying the same procedure for various fault locations (x) and different fault resistances (R_f), the winding protection coverage levels can be determined for the same reduced operating speed of 900 rpm, as shown in Fig. 10. The results indicate that the proposed protection method notably increases the winding protection coverage compared to the conventional approach. In certain cases, the proposed protection can protect the stator winding end with higher potential, where the conventional function fails to do so (e.g. for values of R_f where the auto-adaptive threshold intersects with $U_{gnd,f}$ but the conventional threshold does not). However, for very high fault resistances (in the range of kΩ), neither protection scheme will trigger. Importantly, the proposed method fully addresses the loss of coverage issue discussed in Section II, ensuring that [U_0>] = 5% or α = 95 % is maintained for a solid SGF at any operating speed. As expected, protection coverage decreases with R_f due to the voltage divider in the fault circuit.

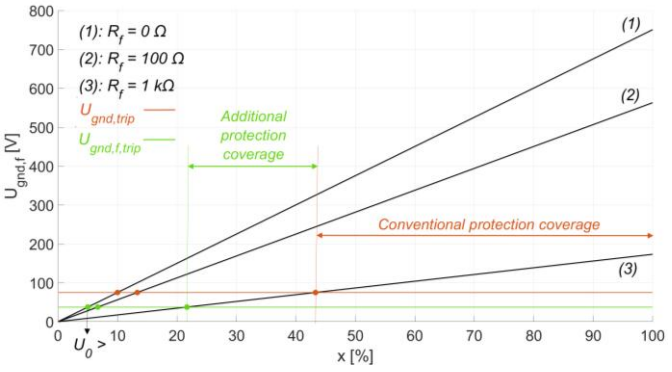

Fig. 10. Simulation results. $U_{gnd,f}$ with respect to the fault location x for different fault resistances R_f under [90 Hz, 1300 V] operating conditions.

If the procedure is extended to various fault locations (x) and fault resistances (R_f), across several off-rated operating speeds (1350, 900, and 450 rpm), the tripping regions can be plotted and analyzed. It is observed that the proposed SGF protection ensures a consistent winding coverage profile as a function of R_f across all operating speeds (geometric locus). This consistency contrasts sharply with conventional schemes, which exhibit a more pronounced reduction in coverage for the same R_f values. Fig.11 illustrates the resulting consistent [x, R_f] protection profile of the proposed method, alongside the corresponding family of [x, R_f] protection profiles for the conventional method, for each operating speed.

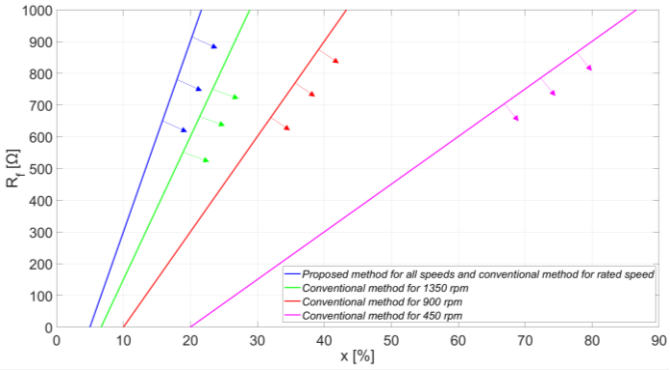

Fig. 11. Simulation results. Geometric locus of [x, R_f] SGF faults under protection for different operating speeds. The arrows point the protected areas.

Consequently, due to the fixed pick-up setting of conventional SGF protection functions, the protection coverage diminishes with the operating speed. For example, as depicted in Fig. 11 for R_f = 300 Ω, α decreases from approximately 90 % to 80 % or 60 % when the operating speed is reduced to half or quarter of its rated value, respectively. The proposed method effectively mitigates the loss of coverage, leading to significantly improved performance, especially at lower speeds.

The simulation results demonstrate that the proposed method significantly improves protection coverage across all off-nominal operating speeds and fault resistance values, with particularly notable enhancements at lower operating speeds and higher fault resistance values, as summarized in Fig. 11.

V. Experimental Tests

A. Experimental Setup

A 3.4-kVA SM was specifically arranged to allow access to several intermediate points along the stator windings, in addition to each winding ends. Detailed nameplate information for this SM, with 2/3 pitch winding, is provided in Table II. The physical arrangement is depicted in Fig. 12. The four intermediate terminals (S1, S2, S3 and S4) on one of the phases enable the execution of SGFs at positions corresponding to x = 2.5, 5, 7.5 and 10% when the neutral is connected to terminals 1, 2 and 3, and symmetrically at x = 97.5, 95, 92.5 and 90% when the neutral is connected to terminals 4, 5 and 6. Since the detection of SGFs becomes trivial when the fault is close to the machine terminals, the neutral point was connected to terminals 1, 2 and 3 for the experimental tests, as the challenge lies in detecting SGFs near the x = *0* end.

The experimental setup, following the schema depicted in Fig. 12, is shown in Fig. 13. The SM operates as a generator,

This work is licensed under a Creative Commons Attribution 4.0 License. For more information, see https://creativecommons.org/licenses/by/4.0/

This article has been accepted for publication in IEEE Transactions on Industry Applications. This is the author's version which has not been fully edited and content may change prior to final publication. Citation information: DOI 10.1109/TIA.2025.3559024

driven by an induction motor that serves as the prime mover, both mounted on the same shaft. The induction motor is powered by the grid through a variable frequency drive (VFD), allowing precise control of the rotational speed and enabling emulation of various operating conditions. The SM's excitation field power is supplied via a DC adjustable source to ensure accurate control of the excitation level under constant flux control. The output of the SM is connected to a three-phase full-wave bridge rectifier and a resistive load, which replicates the power consumption. The load was carefully selected to match the generator's output capabilities, ensuring that the system operates within safe limits.

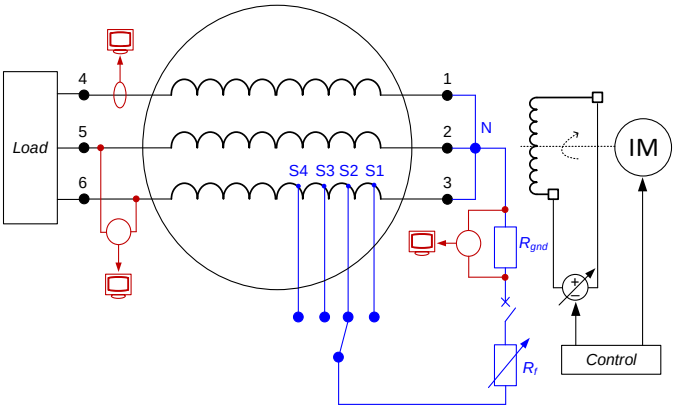

Fig. 12. Experimental setup schema, with accessible stator terminals and fault circuit. Terminals 1 to 6 correspond to winding ends. Terminals S1 to S4 correspond to intermediate points. Terminal N corresponds to the neutral point.

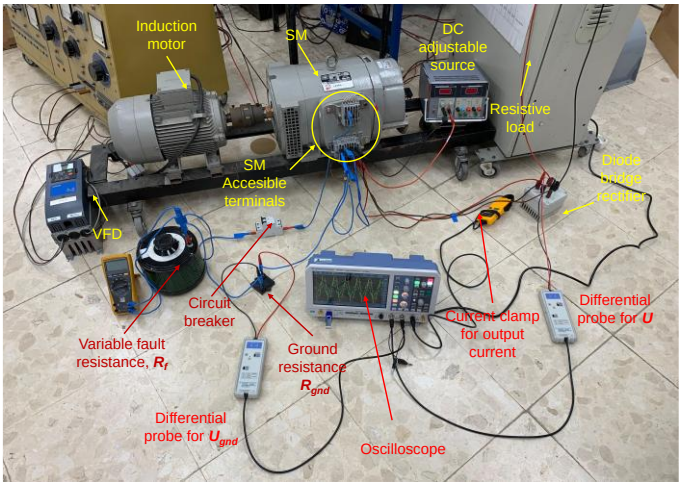

Fig. 13. Experimental setup overview.

TABLE II

TESTED SM NAMEPLATE DATA

Alternator type	Synchronous 3-phase	
Rated power	3.4	kVA
Rated speed	1500	rpm
Rated voltage	400	V
Rated current	5	A
Pole pairs	2	
Rated frequency	50	Hz
IP	21	
Isolation class	F	
Rated excitation voltage	32	V
Rated excitation current	2.90	A
Construction type	B3/B14	

As shown in Fig. 12, a closed-loop fault circuit is established between the machine's neutral and the corresponding fault terminal (S1, S2, S3 or S4). This circuit consists of a fixed-value grounding resistance (R_{gnd} = 46.70 Ω, so as to limit the maximum fault current to 5 A), a variable-value fault resistance (R_f = 0, 11.67, 23.35, 46.70, 58.37, 70.05 or 93.4 Ω), and a circuit breaker, all connected in series. The range of fault resistances was chosen to emulate different fault severities, providing a comprehensive understanding of the protection system's response. When the circuit breaker is closed, the fault loop is activated, short-circuiting the portion of the stator winding between the neutral point and the fault terminal through the specified circuit.

For accurate data acquisition, two differential probes were used to capture the grounding resistor voltage and the machine output line voltage waveforms on the oscilloscope. Additionally, a current clamp was employed to monitor the machine's output current, ensuring it remained below its rated value to prevent overheating and potential damage to the equipment.

B. Experimental Results

The primary objective of the developed setup was to evaluate the performance of the proposed SGF protection method under various fault conditions, with a particular focus on faults occurring near the neutral point, which present the greatest detection challenge. Experimental tests were conducted under different operating conditions, all maintaining constant flux control: [f, U] = [50 Hz, 400 V], [37.5 Hz, 300 V], [25 Hz, 200 V] and [12.5 Hz, 100 V]. In each test, an SGF with fault resistance R_f was performed at an intermediate stator terminal (S1, S2, S3 or S4).

The performance of the proposed protection method was again compared to a benchmark, consisting in the conventional 95 % SGF protection with a fixed setting for 50 Hz, applied under the same tested variable speed conditions. While the resistor voltage tripping threshold, $U_{gnd,f,trip}$, in the proposed protection method is auto-adaptively adjusted according to (4), the conventional protection function uses a fixed threshold, $U_{gnd,trip}$, set according to (2).

A detailed example for an SGF at S3 with R_f = 0 (solid fault) under [25 Hz, 200 V] off-rated operating conditions is depicted in Fig. 14. For [U_o>] = 5%, (4) yields approximately $U_{gnd,f,trip}$ = 5.77 V under these specific operating conditions, while (2) provides approximately $U_{gnd,trip}$ = 11.50 V regardless of the operating conditions. Fig. 14 features the raw voltage signal captured at the grounding resistor terminals, $\underline{U}_{gnd}$, the grounding voltage waveform corresponding to the fundamental frequency (f = 25 Hz) obtained via trailing FFT, $\underline{U}_{gnd,f}$, and its RMS value calculated over a running average window of one cycle of the fundamental frequency, $U_{gnd,f}$.

As shown in Fig. 14, before the SGF is initiated, $\underline{U}_{gnd}$ remains at zero with high-order harmonic noise. As expected, the fundamental harmonic content is negligible, while components above 1 kHz account for more than 84 % of the total power. Following the SGF initiation by closing the fault circuit, a non-zero $\underline{U}_{gnd}$ is impressed across the grounding resistor. This raw signal reaches peak values of 11.31 V and is heavily contaminated by harmonic components, as shown in the FFT window for the cycle of the fundamental frequency indicated in Fig. 14. The results of this FFT are presented in Fig. 15. The signal exhibits a total harmonic distortion (THD) of 12.38 %, calculated with the Nyquist frequency as the maximum

This work is licensed under a Creative Commons Attribution 4.0 License. For more information, see https://creativecommons.org/licenses/by/4.0/

This article has been accepted for publication in IEEE Transactions on Industry Applications. This is the author's version which has not been fully edited and content may change prior to final publication. Citation information: DOI 10.1109/TIA.2025.3559024

frequency. The fundamental frequency component exhibits a peak value of 10.79 V (7.62 V_{RMS}). By converting the time-domain signal into the frequency-domain representation, the contribution of each frequency component to the overall signal is observable in Fig. 15. While the fundamental component accounts for 98.36 % of the signal, the 7th harmonic is the second-largest contributor with 0.81 %, followed by the 5th harmonic with 0.39 %. These harmonic contributions are consistent with a 2/3 pitch winding SM.

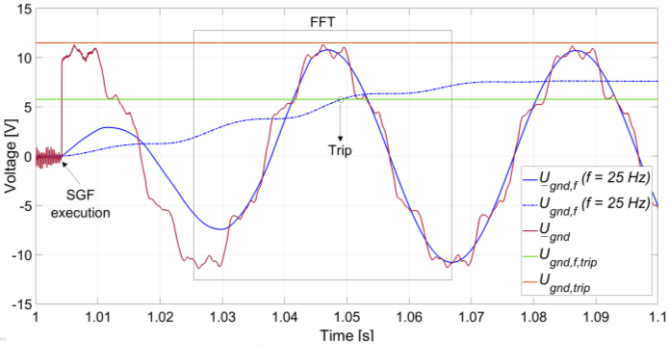

Fig. 14. Experimental results for an SGF at S3 with R_f = 0 (solid fault) under [25 Hz, 200 V] operating conditions.

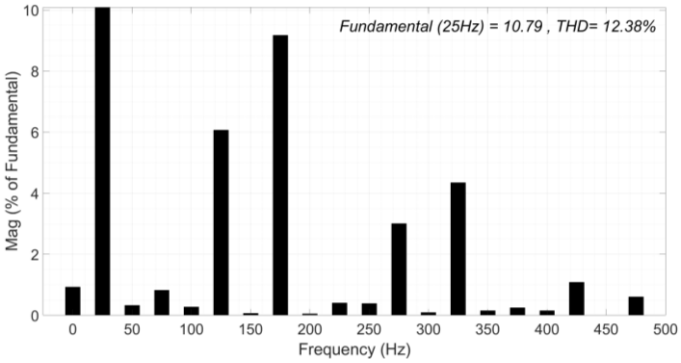

Fig. 15. Experimental results. Bar display of the FFT analysis conducted on $\underline{U}_{gnd}$ after SGF execution, relative to the fundamental frequency under [25 Hz, 200 V] operating conditions

Following the fault initiation, $\underline{U}_{gnd,f}$ stabilizes in both magnitude and phase for the tested SGF after one cycle of the fundamental frequency, due to the trailing window calculation. However, $U_{gnd,f}$ reaches its corresponding steady value after an additional cycle lag. Prior to this calculation lag, the tripping condition described in (5) is satisfied when $U_{gnd,f}$ exceeds $U_{gnd,f,trip}$, which occurs shortly after the first cycle of the fundamental frequency. In contrast, the conventional tripping threshold is set well above the steady value of $U_{gnd,f}$, indicating that the SGF would not be detected by the conventional protection method. The proposed auto-adaptive threshold setting allows to detect SGFs that would remain unnoticed by conventional SGF protection functions, with the same [U_o>] = 5% setting.

Figs. 16, 17 and 18 aggregate the RMS measurements of the grounding resistor voltage ($U_{gnd,f}$) under off-rated operating conditions corresponding to [f, U] = [37.5 Hz, 300 V], [25 Hz, 200 V] and [12.5 Hz, 100 V], respectively, for all the tested R_f values. These figures also show the conventional fixed threshold setting, $U_{gnd,trip}$ = 11.50 V, and the auto-adaptive threshold setting for each operating condition ($U_{gnd,f,trip}$ = 8.66 V, 5.77 V and 2.89 V, for f = 37.5, 25 and 12.5 Hz, respectively). Figs. 16, 17 and 18 illustrate that, due to the fixed pickup setting of conventional SGF protection functions, the protection coverage diminishes as the operating speed decreases. For example, the conventional function only ensures α = 93.36, 90.04 and 80.08 % for a solid SGF at f = 37.5, 25 and 12.5 Hz, respectively. This loss of coverage with speed reduction is avoided with the proposed method. The proposed protection guarantees [U_o>] = 5% or α = 95 % for a solid SGF at any operating speed.

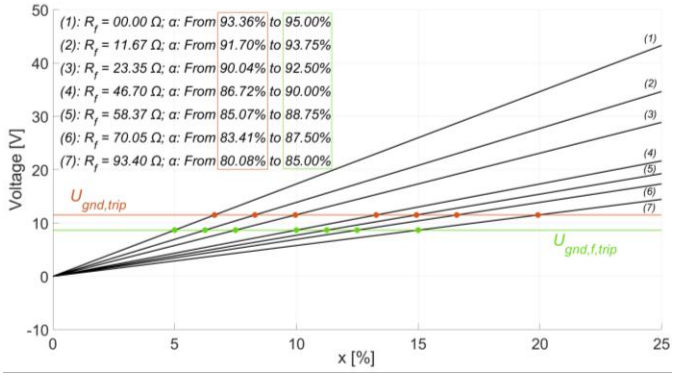

Fig. 16. Experimental results. Grounding resistor voltage at fundamental frequency ($U_{gnd,f}$), as a function of the fault location (x), for f = 37.5 Hz and all tested R_f values, together with conventional ($U_{gnd,trip}$) and auto-adaptive ($U_{gnd,f,trip}$) tripping thresholds. Stator coverage improvements in terms of α[%] are indicated.

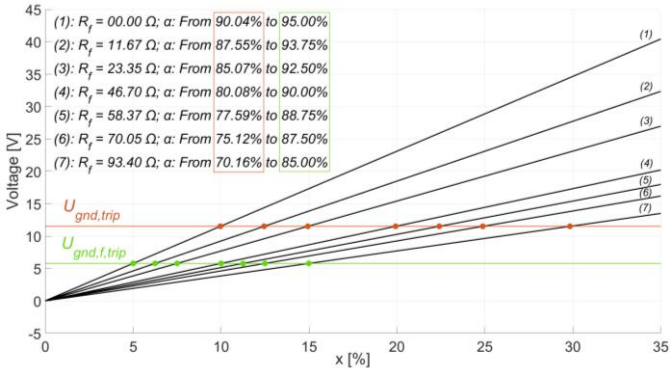

Fig. 17. Experimental results. Grounding resistor voltage at fundamental frequency ($U_{gnd,f}$), as a function of the fault location (x), for f = 25 Hz and all tested R_f values, together with conventional ($U_{gnd,trip}$) and auto-adaptive ($U_{gnd,f,trip}$) tripping thresholds. Stator coverage improvements in terms of α[%] are indicated.

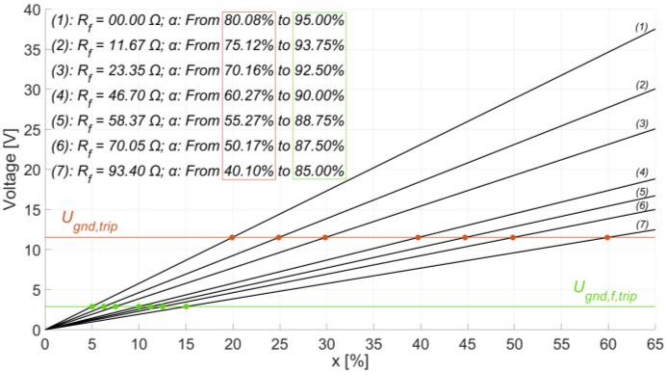

Fig. 18. Experimental results. Grounding resistor voltage at fundamental frequency ($U_{gnd,f}$), as a function of the fault location (x), for f = 12.5 Hz and all tested R_f values, together with conventional ($U_{gnd,trip}$) and auto-adaptive ($U_{gnd,f,trip}$) tripping thresholds. Stator coverage improvements in terms of α[%] are indicated.

This work is licensed under a Creative Commons Attribution 4.0 License. For more information, see https://creativecommons.org/licenses/by/4.0/

This article has been accepted for publication in IEEE Transactions on Industry Applications. This is the author's version which has not been fully edited and content may change prior to final publication. Citation information: DOI 10.1109/TIA.2025.3559024

It is evident from Figs. 16 to 18 that, at each operating speed, the protection coverage decreases for higher R_f values, similar to conventional SGF protection schemes due to the voltage divider effect. In fact, the proposed SGF protection ensures consistent coverage as a function of R_f across all operating speeds: α[%] = [95.00; 93.75; 92.50; 90.00; 88.75; 87.50; 85.00] for R_f[Ω] = [0; 11.67; 23.35; 46.70; 58.37; 70.05; 93.40]. This demonstrates the constant [x, R_f] fault geometric locus for the proposed method regardless of the operating speed. In contrast, the conventional scheme shows a more drastic reduction in coverage for the same R_f values. When analyzing and comparing protection coverage at each operating speed, it is apparent that the decrease in coverage with R_f is more pronounced at lower operating speeds. For example, at f = 37.5 Hz, α drops from 93.36 % to 80.08 % as R_f increases from 0 to 93.40 Ω (Fig. 16), while for f = 12.5 Hz, α falls from 80.08 % to 40.10 % for the same R_f values (Fig. 18). Consequently, the improvement in coverage at lower operating speeds is more significant. For instance, at f = 12.5 Hz and R_f = 93.40 Ω, α improves from 40.10 % to 85 %, more than doubling the stator winding length under protection. These findings demonstrate that the proposed method significantly enhances protection coverage at any off-nominal operating speed and for any fault resistance value, with particularly notable improvements at lower operating speeds and higher fault resistance values.

As stated in Section II, in typical industrial applications, the grounding resistor (R_{gnd}) is usually sized to limit fault currents to 5 or 10 A in the worst-case SGF scenario (R_f = 0 at x = 100 %). This current magnitude is not sufficiently high to cause instantaneous damage to the machine, allowing the protection system to delay its response by a few cycles without compromising safety. This delay enables the system to await the stabilization of the operating frequency, ensuring that the threshold adjustment and fault diagnosis are performed accurately in steady-state conditions. By avoiding the challenges associated with transient noise and instability, this approach enhances the reliability of the proposed method.

VI. Conclusions

In this work, a novel auto-adaptive approach to Stator Ground Fault protection method for SMs operating under variable speed conditions is presented. The proposed approach overcomes the key limitations of conventional fixed-setting protection functions, which struggle to maintain consistent stator winding protection coverage across the operating range. The method dynamically adjusts the tripping threshold of overcurrent or overvoltage schemes based on the machine's operating conditions, ensuring reliable protection off-rated speed operation.

Extensive simulations and experimental tests validate the method's effectiveness, safeguarding up to 95% of the stator winding at any operating speed. The results show significant improvements in fault detection. It is demonstrated that the method ensures a consistent [x, R_f] protection characteristic across all speeds. Therefore, the improvements are particularly greater for high-resistance faults and reduced-speed conditions, where conventional protection schemes lose more coverage or even fail to detect faults.

The proposed method remains simple and cost-effective, avoiding the need for additional equipment or signal injection, as only software developments on conventional relays are required. The auto-adaptive filtering approach based on real-time fundamental frequency tracking from terminal voltage, addresses issues like loss of protection coverage and harmonic miss-filtering that affect fixed-setting methods. Alternative frequency tracking options, such as encoder signals or the drive's PLL frequency setpoint, are also viable.

Future work could extend the auto-adaptive protection method to other machine types, such as induction machines and permanent magnet synchronous machines (PMSMs), enabling wider application in sectors like electric vehicles and aerospace. Additionally, incorporating AI algorithms could enhance fault detection and preventive maintenance by optimizing threshold settings and predicting insulation degradation. Real-time implementation on larger industrial machines, along with hardware optimization using FPGAs or DSPs, would ensure scalability and efficient deployment in industrial settings, reducing latency and computational overhead.

The proposed method is designed to leverage the signal processing capabilities available in modern digital protection relays, which routinely extract fundamental and harmonic components. These functionalities are sufficient to support the adaptive approach proposed in this work without necessitating additional developments in signal processing. However, further advancements in real-time processing techniques represent a promising direction for future research. Exploring techniques such as wavelet analysis could further enhance sensitivity to high-resistance faults.

References

[1] "IEEE Guide for AC Generator Protection," in *IEEE Std C37.102-2023 (Revision of IEEE Std C37.102-2006)*, pp.1-211, 28 June 2024.

[2] N. Klingerman, D. Finney, S. Samineni, N. Fischer and D. Haas, "Understanding generator stator ground faults and their protection schemes," *2016 69th Annual Conference for Protective Relay Engineers (CPRE)*, College Station, TX, USA, 2016, pp. 1-14.

[3] G. C. Stone, E. A. Boulter, I. Culbert and H. Dhirani, Electrical Insulation for Rotating Machines: Design Evaluation Aging Testing and Repair, Hoboken, NJ:Wiley-IEEE Press, 2004.

[4] S. A. Saleh et al., "Experimental Assessment of Grounding System Impacts on Ground Currents and Transient Overvoltage," in *IEEE Transactions on Industry Applications*, vol. 58, no. 5, pp. 5987-6001, Sept.-Oct. 2022.

[5] "IEEE Guide for Generator Ground Protection," in *IEEE Std C37.101-2006 (Revision of IEEE Std C37.101-1993/Incorporates IEEE Std C37.101-2006/Cor1:2007)*, pp.1-70, 15 Nov. 2007.

[6] "IEEE Guide for the Application of Neutral Grounding in Electrical Utility Systems, Part II--Synchronous Generator Systems," in *IEEE Std C62.92.2-2017 (Revision of IEEE Std C62.92.2-1989)*., pp.1-38, 19 May 2017.

[7] C. H. Griffin and J. W. Pope, "Generator Ground Fault Protection Using Overcurrent Overvoltage and Undervoltage Relays", *IEEE Transactions on Power Apparatus and Systems*, vol. PAS-101, no. 12, pp. 4490-4501, Dec. 1982.

[8] J. W. Pope, "A Comparison of 100% Stator Ground Fault Protection Schemes for Generator Stator Windings", *IEEE Transactions on Power Apparatus and Systems*, vol. PAS-103, no. 4, pp. 832-840, April 1984.

[9] S. A. Saleh *et al*., "Testing Ground Fault Protection of Generating Units With Frequency-Selective Grounding," in *IEEE Transactions on Industry Applications*, vol. 59, no. 2, pp. 2400-2412, March-April 2023.

[10] A. Doorwar, B. R. Bhalja and O. P. Malik, "Novel Approach for Synchronous Generator Protection Using New Differential Component," in *IEEE Transactions on Energy Conversion*, vol. 38, no. 1, pp. 180-191, March 2023.

[11] M. Zamani, F. Haghjoo, M. H. Samimi and S. M. A. Cruz, "A Simple Magnetic-Flux-Based Method for Localizing High-Resistance Stator

This work is licensed under a Creative Commons Attribution 4.0 License. For more information, see https://creativecommons.org/licenses/by/4.0/

This article has been accepted for publication in IEEE Transactions on Industry Applications. This is the author's version which has not been fully edited and content may change prior to final publication. Citation information: DOI 10.1109/TIA.2025.3559024

Ground Faults in Synchronous Machines," in *IEEE Transactions on Industrial Electronics*, vol. 71, no. 5, pp. 5253-5262, May 2024.

[12] M. Davarpanah *et al*., "Precise Locating of Stator Winding Earth Fault in Large Synchronous Generators," in *IEEE Transactions on Industry Applications*, vol. 53, no. 3, pp. 3137-3145, May-June 2017.

[13] Y. Wang, X. Yin and Z. Zhang, "The Fault-Current-Based Protection Scheme and Location Algorithm for Stator Ground Fault of a Large Generator," in *IEEE Transactions on Energy Conversion*, vol. 28, no. 4, pp. 871-879, Dec. 2013.

[14] N. Safari-Shad, R. Franklin, A. Negahdari and H. A. Toliyat, "Adaptive 100% Injection-Based Generator Stator Ground Fault Protection With Real-Time Fault Location Capability," in *IEEE Transactions on Power Delivery*, vol. 33, no. 5, pp. 2364-2372, Oct. 2018.

[15] F.R. Blánquez, C.A. Platero, E. Rebollo and F. Blázquez, "On-line stator ground-fault location method for synchronous generators based on 100% stator low-frequency injection protection", *Electric Power Systems Research*, vol. 125, pp. 34-44, Apr. 2015.

[16] J. Qiao, X. Yin, Y. Wang, L. Tan and Q. Lu, "A Precise Stator Ground Fault Location Method for Large Generators Based on Potential Analysis of Slot Conductors," in *IEEE Transactions on Power Delivery*, vol. 37, no. 6, pp. 5203-5213, Dec. 2022.

[17] D. F. Friedemann, D. Motter and R. A. Oliveira, "Stator-Ground Fault Location Method Based on Third-Harmonic Measures in High-Impedance Grounded Generators," in *IEEE Transactions on Power Delivery*, vol. 36, no. 2, pp. 794-802, April 2021.

[18] N. Safari-Shad and R. Franklin, "Adaptive 100% Stator Ground Fault Protection Based on Third-Harmonic Differential Voltage Scheme," in *IEEE Transactions on Power Delivery*, vol. 31, no. 4, pp. 1429-1436, Aug. 2016.

[19] K. Al Jaafari, A. Negahdari, H. A. Toliyat, N. Safari-Shad and R. Franklin, "Modeling and Experimental Verification of a 100% Stator Ground Fault Protection Based on Adaptive Third-Harmonic Differential Voltage Scheme for Synchronous Generators," in *IEEE Transactions on Industry Applications*, vol. 53, no. 4, pp. 3379-3386, July-Aug. 2017.

[20] K. Mahtani, J. M. Guerrero, L. F. Beites and C. A. Platero, "Auto-Adaptive Stator Ground Fault Protection for Synchronous Generators in Diesel-Electric Locomotives," *2023 IEEE 14th International Symposium on Diagnostics for Electrical Machines, Power Electronics and Drives (SDEMPED)*, Chania, Greece, 2023, pp. 116-122.

[21] K. Mahtani, J. M. Guerrero, P.R. Pajarón, L.F. Beites and C.A. Platero, "Método y Sistema de Detección de Faltas a Tierra en el Estátor de una Máquina Síncrona," Spanish Patent ES2953458B2, May 20, 2024.

[22] D. Tierney, B. Kasztenny, D. Finney, D. Haas and B. Le, "Performance of generator protection relays during off-nominal frequency operation," *2014 67th Annual Conference for Pro2tective Relay Engineers*, College Station, TX, USA, 2014, pp. 450-469

BIOGRAPHIES

Kumar Mahtani received his Ph.D. in Electrical Engineering from Universidad Politécnica de Madrid (UPM), Spain in 2023. Previously, he completed his MSc. and BSc. in Electrical Engineering from UPM and Centrale-Supélec (France), in 2020 and 2018 respectively. He works as Assistant Professor at the Department of Electrical Engineering at UPM. His major field of interest include electrical machines diagnostics and protection, and electrical power generation.

José Manuel Guerrero (M'23) received the B.E. in energy resources, fuels and explosive engineering, the M.E. in electrical engineering and the Ph.D. degree in Electrical Engineering from Universidad Politécnica of Madrid, Madrid, Spain, in 2018, 2019, and 2022 respectively. He worked as Assistant Professor at the Department of Energy and Fuels at Universidad Politécnica of Madrid from 2020 to 2023. In 2023, he was professor and lecturer at the Electronics and Computing Department of Mondragon Unibertsitatea. Nowadays, he works in the Department of Electrical Engineering of Universidad del País Vasco as a Researcher Associate Professor where his research field is focused on electric systems protection and fault diagnosis.

Luis F. Beites received the Ph.D. degree in Electrical Engineering in 1999, from Universidad Politécnica de Madrid, Madrid, Spain, where he is currently an Associate Professor. His research interests include electrical power quality, including harmonics, and also the effect of smartgrids, microgrids, HVDCs and all electronics implemented in the network.

Carlos A. Platero (M'10-SM'20) received his Dipl. degree and Ph.D. degree in Electrical Engineering from Universidad Politécnica de Madrid (UPM), Spain, in 1996 and 2007 respectively. From 1996 to 2008 he worked in ABB Generación S.A., Alstom Power S.A. and ENDESA Generación SA, and was involved in the design and commissioning of power plants. In 2002 he started teaching at the Department of Electrical Engineering at UPM, and joined an energy research group. In 2008 he became a Full-time Associate Professor in Electrical Engineering. In 2022 he became a Full-professor in Electrical Engineering. His major field of interest include electrical machines diagnostics and protection, and electrical power generation.

This work is licensed under a Creative Commons Attribution 4.0 License. For more information, see https://creativecommons.org/licenses/by/4.0/